M2AN. MATHEMATICAL MODELLING AND NUMERICAL ANALYSIS
- MODÉLISATION MATHÉMATIQUE ET ANALYSE NUMÉRIQUE

LIN BO ZHANG

# A second-order upwinding finite difference scheme for the steady Navier-Stokes equations in primitive variables in a driven cavity with a multigrid solver

*M2AN. Mathematical modelling and numerical analysis - Modélisation mathématique et analyse numérique*, tome 24, n° 1 (1990), p. 133-150

<http://www.numdam.org/item?id=M2AN_1990__24_1_133_0>

MATHEMATICAL MODELLING AND NUMERICAL ANALYSIS
MODÉLISATION MATHÉMATIQUE ET ANALYSE NUMÉRIQUE
(Vol. 24, n° 1, 1990, p. 133 à 150)

# A SECOND-ORDER UPWINDING FINITE DIFFERENCE SCHEME FOR THE STEADY NAVIER-STOKES EQUATIONS IN PRIMITIVE VARIABLES IN A DRIVEN CAVITY WITH A MULTIGRID SOLVER (*)

Lin Bo ZHANG (1)

Communicated by R. TEMAM

Abstract. — *We present a second-order finite difference scheme for solving the steady navier-Stokes equations in primitive variables in a driven cavity on a staggered grid. The linear terms in the equations are discretized with usual second-order centered differences and the discretization of the nonlinear terms (convection terms) is obtained by a combination of second-order forward and backward differences. This gives a global second-order scheme and ensures numerical stability. The discretized nonlinear system is solved by a multigrid method. Numerical results have been obtained for Reynolds number up to* 10000 *on a* $256 \times 256$ *grid and are in good agreement with those obtained with vorticity-stream function formulations in* [5] *and* [6]. *Comparisons are also made with a classical first-order upwinding scheme.*

Résumé. — *Nous présentons un schéma aux différences finies sur grilles décalées du second ordre pour résoudre les équations de Navier-Stokes stationnaires, dans la cavité entraînée, en formulation vitesse-pression. Les termes linéaires des équations sont discrétisés de façon habituelle et nous proposons un schéma décentré du second ordre pour discrétiser les termes non linéaires de convection. Cela donne globalement un schéma du second ordre qui assure une stabilité numérique. Le système non linéaire obtenu est résolu par une méthode multigrille. Ce schéma nous a permis d'obtenir des résultats numériques pour des nombres de Reynolds élevés jusqu'à* 10000 *sur une grille* $256 \times 256$. *Ces résultats sont en accord avec ceux de* [5] *et* [6] *obtenus avec une formulation vorticité-fonction de courant. Nous les avons également comparés avec ceux obtenus par un schéma classique du premier ordre et décentré.*

(*) Received in May 1988, revised in October 1988.

(1) This paper is a part of the author's works during the preparation of his university thesis at the Laboratoire d'Analyse Numérique d'Orsay, Université Paris-Sud. More detailed descriptions and numerical results can be found in [9].

M² AN Modélisation mathématique et Analyse numérique 0764-583X/90/01/133/18/$ 3.80

## 1. INTRODUCTION

Numerical solution of the Navier-Stokes equations for viscous incompressible flows is always of great interest in fluid dynamics. During recent years efforts have been made to obtain precise numerical solutions for large Reynolds numbers. The difficulties arise with the primitive variables formulation (or $u - p$ formulation) for large reynolds numbers because of the hyperbolic-like behavier of the governing equations, and the treatment of the pression $p$ and the incompressible condition div $u = 0$. The discretization of the nonlinear terms by centered finite differences is unstable when the mesh size is not sufficiently small, while the classical first-order upwinding disfferences is poor in precision. Thus, best numerical results for 2D problems published recently were often obtained with vorticity-stream function formulations.

In this work we study the discretization of the nonlinear terms of the steady Navier-Stokes equations in primitive variables by second-order uncentered finite differences. We use staggered grids in which the first component $u$ of the velocity is discretized in the middle of the two vertical sides of each cell, the second component $v$ in the middle of the two horizontal sides, and the pression $p$ at the center of each cell. Usual centered differences are used for the linear terms in the governing equations and second-order upwindind differences are used for the nonlinear terms. By model problem analysis one can show that the resulting discret nonlinear system is stable for any mesh size and for any Reynolds number (the stability here means there's no numerical oscillation in the solution of the discret system). Multigrid methods (FAS, FMG) are used to solve the discret system, in which we employ the Symetrical Coupled Gauss-Seidel iterations (SCGS), proposed by S. P. Vanka [8], as the smoothing operator. This algorithm is applied to the driven cavity problem which is a classical test problem for numerical solution of the Navier-Stokes equations. Numerical results are obtained for Reynolds numbers up to 10000 on different grids (up to $256 \times 256$), and are compared to those reported in [5], [6], [8], in the case in which the region is the unit square. We present also numerical results obtained in rectangular regions with aspect ratios (height to width ratio) 1 : 2, 4 : 3 and 2 : 1, respectively. Comparisons are also made, in the case of the unit square, with a first-order upwinding scheme for Reynolds number $R = 1\,000$.

Briefly, second-order upwinding finite differences combined with a multigrid solver provides an efficient method for solving the steady Navier-Stokes equations in primitive variables with large Reynolds numbers. This method can also be applied to 3D problems without modification.

## 2. THE GOVERNING EQUATIONS AND THEIR DISCRETIZATION

The 2D steady viscous incompressible flows in a region $\Omega \subset \mathbb{R}^2$ satisfy the steady Navier-Stokes equations :

$$\begin{cases} -\frac{1}{R}\Delta u + u\frac{\partial u}{\partial x} + v\frac{\partial u}{\partial y} + \frac{\partial p}{\partial x} = 0 \\ -\frac{1}{R}\Delta v + u\frac{\partial v}{\partial x} + v\frac{\partial v}{\partial y} + \frac{\partial p}{\partial y} = 0 \\ \frac{\partial u}{\partial x} + \frac{\partial v}{\partial y} = 0 \\ \quad + \text{boundary conditions} \end{cases}$$

where $(u, v)$ is the (nondimensional) velocity, $p$ is the (nondimensional) pression and $R > 0$ is the Reynolds number. $x$, $y$ denote the two space directions.

To discretize these equations, we use a classical staggered grid. Let $h > 0$ be the mesh size. For any function $\phi(x, y)$, $\phi_{j,k}$ denotes $\phi(jh, kh)$ for all $(j, k) \in \mathbb{R}^2$.

We denote by $\Omega_h$ the *reference grid :*

$$\Omega_h = \{(jh, kh) \mid (j, k) \in \mathbf{Z}^2\} \cap \Omega .$$

The grid at which are discretized the first component $u$ of the velocity and the first equation is :

$$\Omega_h^u = \left\{ \left( jh, \left( k + \frac{1}{2} \right) h \right) \middle| (j, k) \in \mathbf{Z}^2 \right\} \cap \Omega .$$

The grid for the second component $v$ of the velocity and the second equation is :

$$\Omega_h^v = \left\{ \left( \left( j + \frac{1}{2} \right) h, kh \right) \middle| (j, k) \in \mathbf{Z}^2 \right\} \cap \Omega .$$

The grid for the pression $p$ and the third equation (the continuity equation) is :

$$\Omega_h^p = \left\{ \left( \left( j + \frac{1}{2} \right) h, \left( k + \frac{1}{2} \right) h \right) \middle| (j, k) \in \mathbf{Z}^2 \right\} \cap \Omega .$$

The linear term of the equations are approximated by usual centered differences. We have :

$$-(\Delta u)_{j,k+\frac{1}{2}} \approx \frac{4\,u_{j,k+\frac{1}{2}} - u_{j-1,k+\frac{1}{2}} - u_{j+1,k+\frac{1}{2}} - u_{j,k-\frac{1}{2}} - u_{j,k+\frac{3}{2}}}{h^2}$$

$$-(\Delta v)_{j+\frac{1}{2},k} \approx \frac{4v_{j+\frac{1}{2},k} - v_{j+\frac{1}{2},k+1} - v_{j+\frac{1}{2},k-1} - v_{j-\frac{1}{2},k} - v_{j+\frac{3}{2},k}}{h^2}$$

$$\left(\frac{\partial p}{\partial x}\right)_{j,k+\frac{1}{2}} \approx \frac{p_{j+\frac{1}{2},k+\frac{1}{2}} - p_{j-\frac{1}{2},k+\frac{1}{2}}}{h}$$

$$\left(\frac{\partial p}{\partial y}\right)_{j+\frac{1}{2},k} \approx \frac{p_{j+\frac{1}{2},k+\frac{1}{2}} - p_{j+\frac{1}{2},k-\frac{1}{2}}}{h}$$

$$\left(\frac{\partial u}{\partial x} + \frac{\partial v}{\partial y}\right)_{j+\frac{1}{2},k+\frac{1}{2}} \approx \frac{u_{j+1,k+\frac{1}{2}} - u_{j,k+\frac{1}{2}} + v_{j+\frac{1}{2},k+1} - v_{j+\frac{1}{2},k}}{h}.$$

For the discretization of the nonlinear terms (or convection terms), we use second-order upwinding differences :

$$\left(u\frac{\partial u}{\partial x}\right)_{j,k+\frac{1}{2}} \approx \begin{cases} u_{j,k+\frac{1}{2}} \dfrac{3u_{j,k+\frac{1}{2}} - 4u_{j-1,k+\frac{1}{2}} + u_{j-2,k+\frac{1}{2}}}{2h}, \\ \qquad\qquad \text{if} \quad u_{j,k+\frac{1}{2}} \geqslant 0 \\ -u_{j,k+\frac{1}{2}} \dfrac{3u_{j,k+\frac{1}{2}} - 4u_{j+1,k+\frac{1}{2}} + u_{j+2,k+\frac{1}{2}}}{2h}, \\ \qquad\qquad \text{if} \quad u_{j,k+\frac{1}{2}} < 0 \end{cases}$$

$$\left(v\frac{\partial u}{\partial y}\right)_{j,k+\frac{1}{2}} \approx \begin{cases} v_{j,k+\frac{1}{2}} \dfrac{3u_{j,k+\frac{1}{2}} - 4u_{j,k-\frac{1}{2}} + u_{j,k-\frac{3}{2}}}{2h}, \\ \qquad\qquad \text{if} \quad v_{j,k+\frac{1}{2}} \geqslant 0 \\ -v_{j,k+\frac{1}{2}} \dfrac{3u_{j,k+\frac{1}{2}} - 4u_{j,k+\frac{3}{2}} + u_{j,k+\frac{5}{2}}}{2h}, \\ \qquad\qquad \text{if} \quad v_{j,k+\frac{1}{2}} < 0 \end{cases}$$

$$\left(u\frac{\partial v}{\partial x}\right)_{j+\frac{1}{2},k} \approx \begin{cases} u_{j+\frac{1}{2},k} \dfrac{3v_{j+\frac{1}{2},k} - 4v_{j-\frac{1}{2},k} + v_{j-\frac{3}{2},k}}{2h}, \\ \qquad\qquad \text{if} \quad u_{j+\frac{1}{2},k} \geqslant 0 \\ -u_{j+\frac{1}{2},k} \dfrac{3v_{j+\frac{1}{2},k} - 4v_{j+\frac{3}{2},k} + v_{j+\frac{5}{2},k}}{2h}, \\ \qquad\qquad \text{if} \quad u_{j+\frac{1}{2},k} < 0 \end{cases}$$

$$\left(v\frac{\partial v}{\partial y}\right)_{j+\frac{1}{2},k} \approx \begin{cases} v_{j+\frac{1}{2},k}\dfrac{3v_{j+\frac{1}{2},k}-4v_{j+\frac{1}{2},k-1}+v_{j+\frac{1}{2},k-2}}{2h}, \\ \qquad\qquad \text{if} \quad v_{j+\frac{1}{2},k}\geqslant 0 \\ -v_{j+\frac{1}{2},k}\dfrac{3v_{j+\frac{1}{2},k}-4v_{j+\frac{1}{2},k+1}+v_{j+\frac{1}{2},k+2}}{2h}, \\ \qquad\qquad \text{if} \quad v_{j+\frac{1}{2},k}<0 \end{cases}$$

where $u_{j+\frac{1}{2},k}$ (respectively $v_{j,k+\frac{1}{2}}$), who is not defined at $\Omega_h^u$ (respectively $\Omega_h^v$), is calculated by bilinear interpolation :

$$u_{j+\frac{1}{2},k} = \frac{1}{4}\left(u_{j,k+\frac{1}{2}} + u_{j+1,k+\frac{1}{2}} + u_{j,k-\frac{1}{2}} - u_{j+1,k-\frac{1}{2}}\right)$$

(respectively,

$$v_{j,k+\frac{1}{2}} = \frac{1}{4}\left(v_{j+\frac{1}{2},k} + v_{j+\frac{1}{2},k+1} + v_{j-\frac{1}{2},k} + v_{j-\frac{1}{2},k+1}\right)\right).$$

This kind of differencing always gives positive contributions to the diagonal of the discret system and thus ensures numerical stability.

Near the boundaries, when points who are not in $\Omega$ have to be used, quadratic extrapolations are employed to calculate function values needed. Boundary conditions should be taken into account in these extrapolations.

### 3. MULTIGRID SOLVER FOR THE DISCRET NONLINEAR SYSTEM

The multigrid methods [2] are based on the fact that most classical iterative methods for solving a system of algebraic equations (obtained by discretization of differential equations), typically the Gauss-Seidel method, the Jacobi method and the $LU$ incomplet decomposition method, reduce rapidly high frequency components of the error function (those whose wavelength is comparable to the mesh size of the grid used in the discretization), while the convergence is slowed down only by low frequency components in the error function. Because low frequency components of a function can be well represented by discretizations on coarse grids, by combining several grids of different mesh size, we can eliminate each sequence of error components at corresponding grid with a same iterative method and obtain rapid convergence. The iterative method used to smooth out solutions on each grid is called smoothing operator. For a review of the multigrid methods and their application to elliptic flow problems, we refer to [2].

In present implementation, we use both FAS and FMG schemes. A sequence of mesh sizes $h_0, \ldots, h_K$ such that $h_{l+1} = \dfrac{h_l}{2}$ is used to produce a

sequence of grids. The restriction and prolongation operators are constructed by either local averagings or bilinear interpolations (so they are all of second-order). The high-order interpolation operator used in FMG to compute an initial approximation on a grid from the solution calculated on a coarser grid is obtained by cibubic interpolations (or extrapolations near the boundaries) for the velocity and biquadratic interpolations (or extrapolations) for the pression.

For the smoothing operator, we have chosen the Symetrical Coupled Gauss-Seidel iterations (SCGS), proposed by S. P. Vanka [8]. For describing this method, we take a cell $\{(jh, kh), ((j+1)h, kh), ((j+1)h, (k+1)h), (jh, (k+1)h)\}$ of the reference grid $\Omega_h$. Four velocities $(u_{j,k+\frac{1}{2}}, u_{j+1,k+\frac{1}{2}}, v_{j+\frac{1}{2},k}, v_{j+\frac{1}{2},k+1})$, one pression $(p_{j+\frac{1}{2},k+\frac{1}{2}})$ and five corresponding equations are defined in this cell. The four momentum equations are linearized by replacing the coefficients of the nonlinear terms by their actual approximation. In each momentum equation, only the velocity component defined at the corresponding point and the pression defined in the current cell are considered as unknowns and all other variables are replaced by their actual approximation. In the continuity equation, all variables defined in the current cell are taken as unknowns. We can write these five equations in the following form :

$$\frac{4\tilde{u}_{j,k+\frac{1}{2}} - u_{j-1,k+\frac{1}{2}} - u_{j+1,k+\frac{1}{2}} - u_{j,k-\frac{1}{2}} - u_{j,k+\frac{3}{2}}}{Rh^2} +$$

$$+ \frac{\tilde{p}_{j+\frac{1}{2},k+\frac{1}{2}} - p_{j-\frac{1}{2},k+\frac{1}{2}}}{h}$$

$$+ \left|u_{j,k+\frac{1}{2}}\right| \frac{3\tilde{u}_{j,k+\frac{1}{2}} - 4u_{j\mp1,k+\frac{1}{2}} + u_{j\mp2,k+\frac{1}{2}}}{2h}$$

$$+ \left|v_{j,k+\frac{1}{2}}\right| \frac{3\tilde{u}_{j,k+\frac{1}{2}} - 4u_{j,k+\frac{1}{2}\mp1} + u_{j,k+\frac{1}{2}\mp2}}{2h} = 0$$

$$\frac{4\tilde{u}_{j+1,k+\frac{1}{2}} - u_{j,k+\frac{1}{2}} - u_{j+2,k+\frac{1}{2}} - u_{j+1,k-\frac{1}{2}} - u_{j+1,k+\frac{3}{2}}}{Rh^2} +$$

$$+ \frac{p_{j+\frac{3}{2},k+\frac{1}{2}} - \tilde{p}_{j+\frac{1}{2},k+\frac{1}{2}}}{h}$$

$$+ \left|u_{j+1,k+\frac{1}{2}}\right| \frac{3\tilde{u}_{j+1,k+\frac{1}{2}} - 4u_{j+1\mp1,k+\frac{1}{2}} + u_{j+1\mp2,k+\frac{1}{2}}}{2h} +$$

$$+ \left|v_{j+1,k+\frac{1}{2}}\right| \frac{3\,\tilde{u}_{j+1,k+\frac{1}{2}} - 4\,u_{j+1,k+\frac{1}{2}\mp 1} + u_{j+1,k+\frac{1}{2}\mp 2}}{2h} = 0$$

$$\frac{4\,\tilde{v}_{j+\frac{1}{2},k} - v_{j+\frac{1}{2},k-1} - v_{j+\frac{1}{2},k+1} - v_{j-\frac{1}{2},k} - v_{j+\frac{3}{2},k}}{Rh^2} +$$

$$+ \frac{\tilde{p}_{j+\frac{1}{2},k+\frac{1}{2}} - p_{j+\frac{1}{2},k-\frac{1}{2}}}{h}$$

$$+ \left|u_{j+\frac{1}{2},k}\right| \frac{3\,\tilde{v}_{j+\frac{1}{2},k} - 4\,v_{j+\frac{1}{2}\mp 1,k} + v_{j+\frac{1}{2}\mp 2,k}}{2h}$$

$$+ \left|v_{j+\frac{1}{2},k}\right| \frac{3\,\tilde{v}_{j+\frac{1}{2},k} - 4\,v_{j+\frac{1}{2},k\mp 1} + v_{j+\frac{1}{2},k\mp 2}}{2h} = 0$$

$$\frac{4\,\tilde{v}_{j+\frac{1}{2},k+1} - v_{j+\frac{1}{2},k} - v_{j+\frac{1}{2},k+2} - v_{j-\frac{1}{2},k+1} - v_{j+\frac{3}{2},k+1}}{Rh^2} +$$

$$+ \frac{p_{j+\frac{1}{2},k+\frac{3}{2}} - \tilde{p}_{j+\frac{1}{2},k+\frac{1}{2}}}{h}$$

$$+ \left|u_{j+\frac{1}{2},k+1}\right| \frac{3\,\tilde{v}_{j+\frac{1}{2},k+1} - 4\,v_{j+\frac{1}{2}\mp 1,k+1} + v_{j+\frac{1}{2}\mp 2,k+1}}{2h}$$

$$+ \left|v_{j+\frac{1}{2},k+1}\right| \frac{3\,\tilde{v}_{j+\frac{1}{2},k+1} - 4\,v_{j+\frac{1}{2},k+1\mp 1} + v_{j+\frac{1}{2},k+1\mp 2}}{2h}$$

$$+ \frac{\tilde{u}_{j+1,k+\frac{1}{2}} - \tilde{u}_{j,k+\frac{1}{2}} + \tilde{v}_{j+\frac{1}{2},k+1} - \tilde{v}_{j+\frac{1}{2},k}}{h} = 0$$

where variables with a « ~ » are considered as unknowns.

This gives us a system of linear equations with five unknowns. We can write this system in the following form :

$$\begin{pmatrix} * & 0 & 0 & 0 & * \\ 0 & * & 0 & 0 & * \\ 0 & 0 & * & 0 & * \\ 0 & 0 & 0 & * & * \\ * & * & * & * & 0 \end{pmatrix} \begin{pmatrix} \tilde{u}_{j,k+\frac{1}{2}} \\ \tilde{u}_{j+1,k+\frac{1}{2}} \\ \tilde{v}_{j+\frac{1}{2},k} \\ \tilde{v}_{j+\frac{1}{2},k+1} \\ \tilde{p}_{j+\frac{1}{2},k+\frac{1}{2}} \end{pmatrix} = \begin{pmatrix} * \\ * \\ * \\ * \\ * \end{pmatrix}.$$

It is solved by a direct method. Because of the nonlinearity of the original system, the new approximations obtained are underrelaxed by :

$$\begin{cases} \tilde{\tilde{u}}_{j,k+\frac{1}{2}} = u_{j,k+\frac{1}{2}} + \beta(\tilde{u}_{j,k+\frac{1}{2}} - u_{j,k+\frac{1}{2}}) \\ \tilde{\tilde{u}}_{j+1,k+\frac{1}{2}} = u_{j+1,k+\frac{1}{2}} + \beta(\tilde{u}_{j+1,k+\frac{1}{2}} - u_{j+1,k+\frac{1}{2}}) \\ \tilde{\tilde{v}}_{j+\frac{1}{2},k} = v_{j+\frac{1}{2},k} + \beta(\tilde{v}_{j+\frac{1}{2},k} - v_{j+\frac{1}{2},k}) \\ \tilde{\tilde{v}}_{j+\frac{1}{2},k+1} = v_{j+\frac{1}{2},k+1} + \beta(\tilde{v}_{j+\frac{1}{2},k+1} - v_{j+\frac{1}{2},k+1}) \end{cases}$$

where $\beta$ is a underrelaxation parameter ($\beta \in (0, 1)$).

$\tilde{\tilde{u}}_{j,k+\frac{1}{2}}$, $\tilde{\tilde{u}}_{j+1,k+\frac{1}{2}}$, $\tilde{\tilde{v}}_{j+\frac{1}{2},k}$, $\tilde{\tilde{v}}_{j+\frac{1}{2},k+1}$ and $\tilde{\tilde{p}}_{j+\frac{1}{2},k+\frac{1}{2}}$ are taken as new approximations to the corresponding variables. All cells in $\Omega_h$ are scanned successively in certain order. One such sweep is called an SCGS iteration.

This method has been applied as smoothing operator to the steady Navier-Stokes equations discretized by a hybrid finite difference scheme (combination of centered and first-order upwinding differences) by Vanka [8] and has been shown to have rapid convergence, especially for large Reynolds numbers. Our numerical experience showed that it is also an efficient smoothing operator for the second-order upwinding finite difference scheme.

## 4. NUMERICAL RESULTS FOR FLOWS IN A DRIVEN CAVITY

We apply the second-order upwinding finite difference scheme to the driven cavity problem. It concerns flows in a rectangular region with the top side moving at a constant velocity. The boundary conditions are described by figure 1. This is a model problem for testing the efficiency of numerical schemes in fluid dynamics. Many results for this problem obtained with different formulations and different methods have been published. But until recently, these results were not accurate for large Reynolds numbers ($\geqslant 400$). Most calculations were made with stream function-vorticity formulations. Best results obtained with the velocity-pression formulation for Reynolds numbers up to 2000 were probably those reported by S. P. Vanka in [8], who used a hybrid finite difference scheme on the convection terms (combination of first-order upwinding and second-order centered differences) and a multigrid solver.

Since we have not yet studied the optimal implementation of the multigrid solver, we are not going to discuss the efficiency of the multigrid solver. Our

principal objective here is to present quantitative results obtained with the second-order upwinding scheme. We mention only that the computations with the second-order upwinding scheme take no many more CPU times than with a classical first-order upwinding scheme (obtained by replacing the second-order upwinding differences by first-order upwinding differences in the discretization of the convection terms) and with the same multigrid solver.

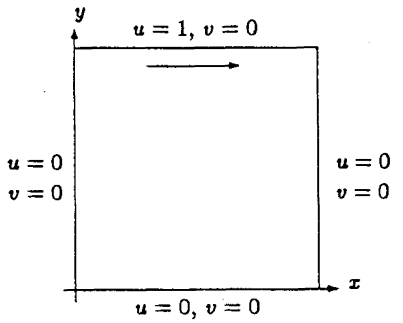


**Figure 1. — Boundary conditions of the driven cavity problem.**

### 4.1. Case of a Square Cavity

Consider the case in which the computational region is the unit square $(0, 1) \times (0, 1)$. The control of passages between different grids in the FAS algorithm is identical to that used in Vanka [8]. The finest grid used is $256 \times 256$ and the coarsest one is $2 \times 2$. The underrelaxation parameter $\beta$ is set to 1 for $R = 100$ and 0.1 for $R = 10\,000$.

We are especially interested in the extrema of $u$ and $v$ velocities along the geometric (vertical and horizontal) centerlines of the cavity, the location of the center of the three principal vortices and the corresponding value of the stream function $\Psi$ at these centers, on which many comparable results have been published. These vortices are the central vortex (called principal vortex), the most important vortex in the lower-left corner of the cavity (called left subvortex) and the most important vortex in the lower-left corner of the cavity (called left subvortex) and the most important vortex in lower-right corner (called right subvortex).

#### 4.1.1. *Comparisons with a First-order Upwinding Scheme*

We first compare numerical results with those obtained by a classical first-order upwinding scheme in which the discretization of the nonlinear terms is

replaced by first-order upwinding finite differences. For example, the term $u\frac{\partial u}{\partial x}$ is discretized by :

$$\left(u\frac{\partial u}{\delta x}\right)_{j,k+\frac{1}{2}} \approx \begin{cases} u_{j,k+\frac{1}{2}}\dfrac{u_{j,k+\frac{1}{2}} - u_{j-1,k+\frac{1}{2}}}{h}, & \text{if } u_{j,k+\frac{1}{2}} \geqslant 0 \\ -u_{j,k+\frac{1}{2}}\dfrac{u_{j,k+\frac{1}{2}} - u_{j+1,k+\frac{1}{2}}}{h}, & \text{if } u_{j,k+\frac{1}{2}} < 0 . \end{cases}$$

The resulted discret system is solved by the same multigrid solver.

Table 1 gives the underrelaxation parameter β and corresponding CPU times. The computations are effectuated with the FMG scheme. The convergence criterion is fixed at $10^{-4}$ on the residu of the discret system (in $L^2$ norm). The CPU times given in the table are those on an SPS-7 (whose executing speed is about 1/50 of that of IBM 3090).

TABLE 1

*Relaxation parameter and* CPU *times.*

| | First-order scheme | | | | Second-order scheme | | | |
|---|---|---|---|---|---|---|---|---|
| | | CPU times (seconds) | | | | CPU times (seconds) | | |
| $R$ | $\beta$ | $h = 1/64$ | $h = 1/128$ | $h = 1/256$ | $\beta$ | $h = 1/64$ | $h = 1/128$ | $h = 1/256$ |
| 100 | 1.1 | 253 | 955 | 4632 | 1.0 | 256 | 951 | 3836 |
| 400 | 0.55 | 373 | 1399 | 5372 | 0.70 | 395 | 1057 | 4028 |
| 1000 | 0.52 | 570 | 1795 | 5709 | 0.60 | 1277 | 2236 | 4767 |
| 2000 | 0.48 | 721 | 2054 | 6381 | 0.55 | 2441 | 4379 | 7995 |
| 3200 | 0.37 | 997 | 3399 | 9196 | 0.60 | 5235 | 7384 | 9911 |

TABLE 2

*Center of principal vortices and corresponding value of* $\Psi$, $R = 1\,000$.

| First-order scheme | | | | | | |
|---|---|---|---|---|---|---|
| | principal vortex | | left subvortex | | right subvortex | |
| grid | $\Psi$ | location | $\Psi$ | location | $\Psi$ | location |
| 32 | 6.991$E$−02 | (0.5938, 0.6563) | −6.77$E$−06 | (0.0625, 0.0313) | −5.37$E$−04 | (0.8750, 0.1563) |
| 64 | 9.881$E$−02 | (0.5469, 0.5859) | −7.94$E$−05 | (0.0781, 0.0625) | −1.14$E$−03 | (0.8750, 0.1172) |
| 128 | 9.881$E$−02 | (0.5469, 0.5859) | −7.94$E$−05 | (0.0781, 0.0625) | −1.14$E$−03 | (0.8750, 0.1172) |
| 256 | 1.071$E$−01 | (0.5391, 0.5742) | −1.33$E$−04 | (0.0781, 0.0703) | −1.39$E$−03 | (0.8711, 0.1133) |
| Second-order scheme | | | | | | |
| | principal vortex | | left subvortex | | right subvortex | |
| grid | $\Psi$ | location | $\Psi$ | location | $\Psi$ | location |
| 32 | 1.216$E$−01 | (0.5313, 0.5938) | −3.14$E$−04 | (0.0938, 0.0938) | −2.27$E$−03 | (0.8125, 0.1250) |
| 64 | 1.212$E$−01 | (0.5313, 0.5625) | −2.22$E$−04 | (0.0781, 0.0781) | −1.83$E$−03 | (0.8438, 0.1094) |
| 128 | 1.199$E$−01 | (0.5313, 0.5625) | −2.35$E$−04 | (0.0859, 0.0781) | −1.77$E$−03 | (0.8594, 0.1094) |
| 256 | 1.193$E$−01 | (0.5313, 0.5664) | −2.35$E$−04 | (0.0820, 0.0781) | −1.74$E$−03 | (0.8633, 0.1133) |

In table 2, we give the location of the center of the three major vortices and the corresponding value of the stream function $\Psi$, for $R = 1\,000$, computed on different grids.

Figures 2-5 show the profiles of the velocity on the geometrical centerlines of the cavity computed on several grids.

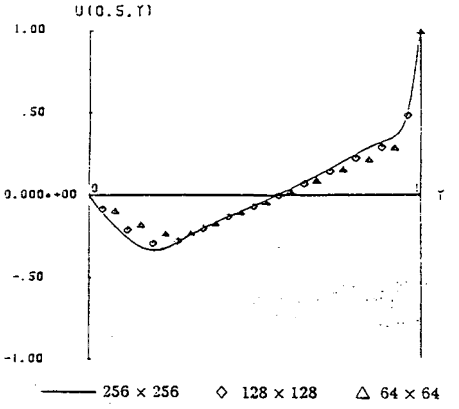


Figure 2. — *u*-velocity along vertical centerline for $R = 1\,000$ obtained on grids 64 × 64, 128 × 128 and 256 × 256 with the first-order scheme.

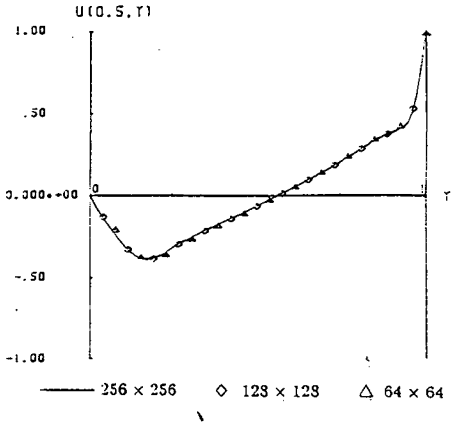


Figure 3. — *u*-velocity along vertical centerline for $R = 1\,000$ obtained on grids 64 × 64, 128 × 128 and 256 × 256 with the second-order scheme.

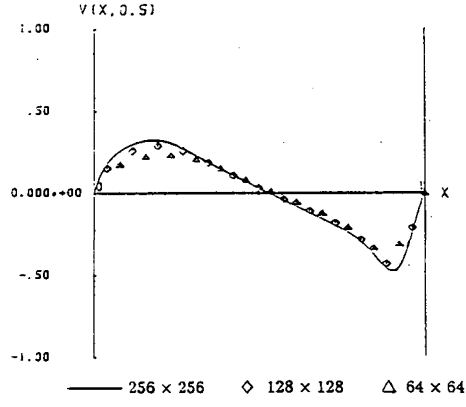


Figure 4. — *v*-velocity along horizontal centerline for $R = 1\,000$ obtained on grids 64 × 64, 128 × 128 and 256 × 256 with the first-order scheme.

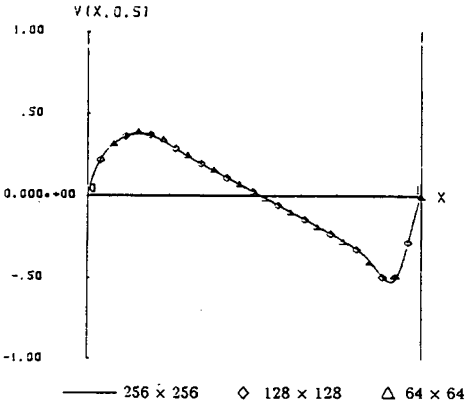


Figure 5. — *v*-velocity along horizontal centerline for $R = 1\,000$ obtained on grids 64 × 64, 128 × 128 and 256 × 256 with the second-order scheme.

From these tables and figures we see that the second-order upwinding scheme takes no many more CPU times than the corresponding first-order upwinding scheme but gives many more accurate results.

4.1.2. *Numerical results and Comparisons with Other Auhors*

At present time, the structure of flows in a square cavity is already well-known. So we present our results without comment. These results are obtained on the $256 \times 256$ grid with the second-order upwinding scheme and the FMG solver. They are summarized in Tables 3-4 and figures 6-11. Also given in the tables the corresponding results obtained by U. Ghia *et al.* [5], R. Schreiber & H. B. Keller [6] and S. P. Vanka [8].

TABLE 3

*Minimum value of u-velocity on the vertical centerline and minimum & maximum values of v-velocity on the horizontal centerline.* a) *this work ;* b) *Ghia et al.* [5] ; c) *Vanka* [8] ;

| $R$ | | $u_{min}$ , $y_{min}$ | $v_{max}$ , $x_{max}$ | $v_{min}$ , $x_{min}$ |
|---|---|---|---|---|
| 100 | a) | −0.21411 , 0.45898 | 0.17964, 0.23633 | −0.25391, 0.81055 |
| | b) | −0.21090 , 0.4531 | 0.17527, 0.2344 | −0.24533, 0.8047 |
| | c) | −0.21300 , 0.4578 | — | — |
| 400 | a) | −0.32926 , 0.27930 | 0.30433, 0.22461 | −0.45455, 0.86133 |
| | b) | −0.32726 , 0.2813 | 0.30203, 0.2266 | −0.44993, 0.8594 |
| | c) | −0.32700 , 0.2797 | — | — |
| 1000 | a) | −0.39009 , 0.16992 | 0.37847, 0.15820 | −0.52839, 0.90820 |
| | b) | −0.38289 , 0.1719 | 0.37095, 0.1563 | −0.51550, 0.9063 |
| | c) | −0.38700 , 0.1734 | — | — |
| 2000 | a) | −0.42289 , 0.11914 | 0.41706, 0.11914 | −0.55846, 0.93555 |
| | c) | −0.41500 , 0.1203 | — | — |
| 3200 | a) | −0.44006 , 0.09180 | 0.43814, 0.09570 | −0.57228, 0.94727 |
| | b) | −0.41933 , 0.1016 | 0.42768, 0.0938 | −0.54053, 0.9453 |
| 5000 | a) | −0.45347 , 0.07617 | 0.45558, 0.08008 | −0.58091, 0.95508 |
| | b) | −0.43643 , 0.0703 | 0.43648, 0.0781 | −0.55408, 0.9531 |
| | c) | −0.33500 , 0.08437 | — | — |
| 7500 | a) | −0.46413 , 0.06445 | 0.47129, 0.06836 | −0.58878, 0.96289 |
| | b) | −0.43590 , 0.0625 | 0.44030, 0.0703 | −0.55216, 0.9609 |
| 10000 | a) | −0.47512 , 0.05664 | 0.48774, 0.06055 | −0.59495, 0.96680 |
| | b) | −0.42735 , 0.0547 | 0.43983, 0.0625 | −0.54302, 0.9688 |

## 4.2. Flows in Rectangular Cavities

The computational region is the rectangle $(O, A) \times (O, B)$ with $A \neq B$. Few results have been published for this problem and none of them was accurate enough to be quantitative. So numerical results presented here can be used for later comparisons.

TABLE 4

*Location of the center of principal vortices and corresponding value of* $\Psi$.
a) *this work ;* b) *Ghia et al.* [5] ; c) *Vanka* [8] ; d) *Schreiber & Keller* [6].

| | | principal vortex | | left subvortex | | right subvortex | |
|---|---|---|---|---|---|---|---|
| $R$ | | $\Psi$ | location | $\Psi$ | location | $\Psi$ | location |
| 100 | a) | $1.035E-1$ | (0.6172, 0.7383) | $-1.80E-6$ | (0.0352, 0.0352) | $-1.28E-5$ | (0.9414, 0.0625) |
| | b) | $1.034E-1$ | (0.6172, 0.7344) | $-1.75E-6$ | (0.0313, 0.0391) | $-1.25E-5$ | (0.9453, 0.0625) |
| | c) | $1.034E-1$ | (0.6188, 0.7375) | $-1.94E-6$ | (0.0375, 0.0313) | $-1.14E-5$ | (0.9375, 0.0563) |
| | d) | $1.033E-1$ | (0.6167, 0.7417) | $-2.05E-6$ | (0.0333, 0.0250) | $-1.32E-5$ | (0.9417, 0.0500) |
| 400 | a) | $1.141E-1$ | (0.5547, 0.6055) | $-1.44E-5$ | (0.0508, 0.0469) | $-6.48E-4$ | (0.8867, 0.1250) |
| | b) | $1.139E-1$ | (0.5547, 0.6055) | $-1.42E-5$ | (0.0508, 0.0469) | $-6.42E-4$ | (0.8906, 0.1250) |
| | c) | $1.136E-1$ | (0.5563, 0.6000) | $-1.46E-5$ | (0.0500, 0.0500) | $-6.45E-4$ | (0.8875, 0.1188) |
| | d) | $1.140E-1$ | (0.5571, 0.6071) | $-1.45E-5$ | (0.0500, 0.0429) | $-6.44E-4$ | (0.8857, 0.1143) |
| 1000 | a) | $1.193E-1$ | (0.5313, 0.5664) | $-2.35E-4$ | (0.0820, 0.0781) | $-1.74E-3$ | (0.8633, 0.1133) |
| | b) | $1.179E-1$ | (0.5313, 0.5625) | $-2.31E-4$ | (0.0859, 0.0781) | $-1.75E-3$ | (0.8594, 0.1094) |
| | c) | $1.173E-1$ | (0.5438, 0.5625) | $-2.24E-4$ | (0.075, 0.0813) | $-1.74E-3$ | (0.8625, 0.1063) |
| | d) | $1.189E-1$ | (0.5286, 0.5643) | $-2.17E-4$ | (0.0857, 0.0714) | $-1.70E-3$ | (0.8643, 0.1071) |
| 2000 | a) | $1.217E-1$ | (0.5195, 0.5469) | $-7.48E-4$ | (0.0859, 0.1016) | $-2.50E-3$ | (0.8438, 0.0977) |
| | c) | $1.116E-1$ | (0.5250, 0.5500) | $-6.90E-4$ | (0.0875, 0.1063) | $-2.60E-3$ | (0.8375, 0.0938) |
| 3200 | a) | $1.230E-1$ | (0.5156, 0.5391) | $-1.10E-3$ | (0.0820, 0.1172) | $-2.84E-3$ | (0.8242, 0.0859) |
| | b) | $1.204E-1$ | (0.5165, 0.5469) | $-9.78E-4$ | (0.0859, 0.1094) | $-3.14E-3$ | (0.8125, 0.0859) |
| 4000 | a) | $1.234E-1$ | (0.5156, 0.5391) | $-1.24E-3$ | (0.0781, 0.1250) | $-2.96E-3$ | (0.8086, 0.0781) |
| | d) | $1.220E-1$ | (0.5188, 0.5375) | $-1.12E-3$ | (0.0813, 0.1188) | $-2.80E-3$ | (0.8188, 0.0750) |
| 5000 | a) | $1.240E-1$ | (0.5156, 0.5352) | $-1.35E-3$ | (0.0742, 0.1328) | $-3.06E-3$ | (0.8008, 0.0742) |
| | b) | $1.190E-1$ | (0.5117, 0.5352) | $-1.36E-3$ | (0.0703, 0.1367) | $-3.08E-3$ | (0.8086, 0.0742) |
| | c) | $0.920E-1$ | (0.5125, 0.5313) | $-1.67E-3$ | (0.0625, 0.1563) | $-5.49E-3$ | (0.8500, 0.0813) |
| 7500 | a) | $1.253E-1$ | (0.5117, 0.5313) | $-1.48E-3$ | (0.0625, 0.1523) | $-3.16E-3$ | (0.7813, 0.0664) |
| | b) | $1.200E-1$ | (0.5117, 0.5322) | $-1.47E-3$ | (0.0645, 0.1504) | $-3.28E-3$ | (0.7813, 0.0625) |
| 10000 | a) | $1.265E-1$ | (0.5117, 0.5313) | $-1.51E-3$ | (0.0586, 0.1602) | $-3.08E-3$ | (0.7578, 0.0586) |
| | b) | $1.197E-1$ | (0.5117, 0.5333) | $-1.52E-3$ | (0.0586, 0.1641) | $-3.42E-3$ | (0.7656, 0.0586) |
| | d) | $1.229E-1$ | (0.5140, 0.5307) | — | — | $-2.96E-3$ | (0.7877, 0.0615) |

Three cases are considered :

Case 1 : $A = 1$, $B = 0.5$ on the $160 \times 80$ grid
Case 2 : $A = 0.75$, $B = 1$ on the $96 \times 160$ grid
Case 3 : $A = 0.5$, $B = 1$ on the $80 \times 160$ grid

Only the FAS scheme is implemented in which the $V$-cycle is used with 2 pre-relaxations and 1 post-relaxation on each grid. The SCGS iterations are effectuated in a symetric way : each iteration contains two sweeps on the cells of the reference grid with the first one in alphabetical order and the second one in the reverse order. The coarsest grid is $10 \times 5$, $3 \times 5$ and $5 \times 10$ respectively for the 3 cases.

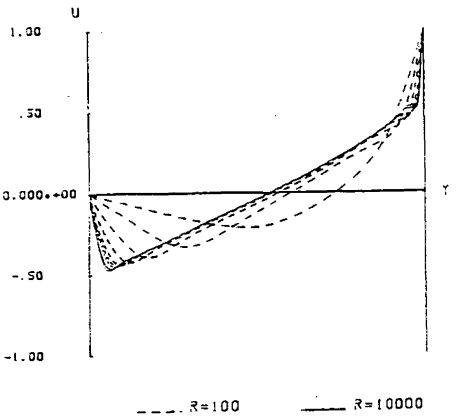


Figure 6. — $u$-velocity along vertical centerline for $R = 100$, 400, 1 000, 2 000, 3 200, 4 000, 5 000, 7 500, 10 000.

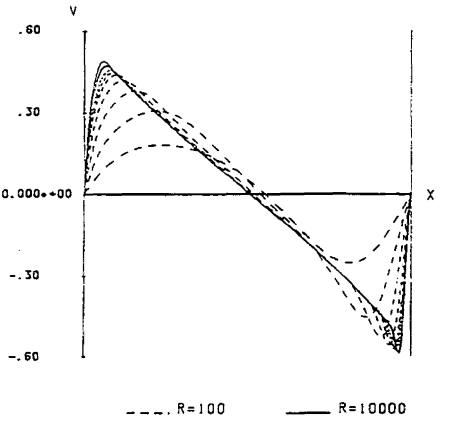


Figure 7. — $v$-velocity along horizontal centerline for $R = 100$, 400, 1 000, 2 000, 3 200, 4 000, 5 000, 7 500, 10 000.

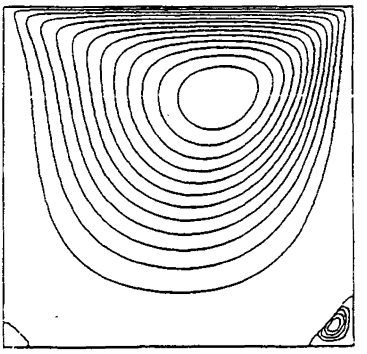

Figure 8. — Streamlines, $R = 100$.

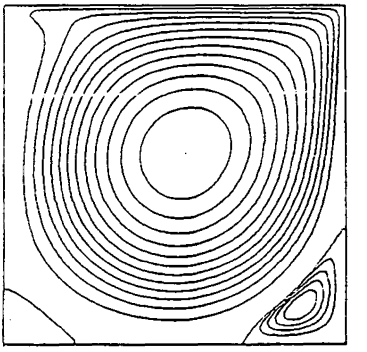

Figure 9 : Streamlines, $R = 1\,000$.

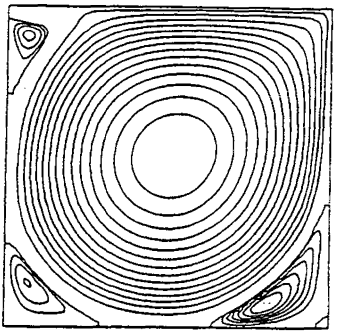

Figure 10 : Streamlines, $R = 5\,000$.

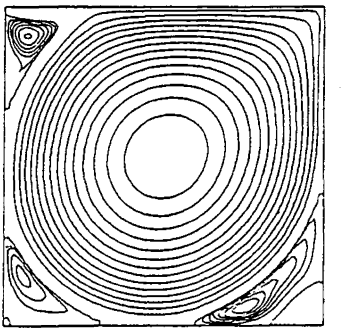

Figure 11 : Streamlines, $R = 10\,000$.

We give numerical results for $R = 100$, 1 000 and 5 000. The underrelaxation parameter $\beta$, the number of $V$-cycles performed, the final residu (in $L^2$ norm) of the discret equation and the CPU time for each $V$-cycle (on an SPS-7) are summarized in table 5.

TABLE 5

*Underrelaxation parameter* $\beta$, *number of V-cycles performed, final residu and required* CPU *time per* MG *iteration.*

| $R$ | | $\beta$ | MG cycles | final residu | CPU time/it |
|---|---|---|---|---|---|
| 100 | case 1 | 1.0 | 5 | 4.88E–5 | 253 secs |
| | case 2 | 1.0 | 5 | 6.47E–5 | 302 secs |
| | case 3 | 1.0 | 5 | 2.25E–5 | 252 secs |
| 1000 | case 1 | 0.6 | 22 | 9.35E–5 | 256 secs |
| | case 2 | 0.6 | 16 | 9.56E–5 | 303 secs |
| | case 3 | 0.6 | 16 | 9.45E–5 | 258 secs |
| 5000 | case 1 | 0.1 | 299 | 9.98E–5 | 266 secs |
| | case 2 | 0.15 | 256 | 9.87E–5 | 318 secs |
| | case 3 | 0.15 | 169 | 9.76E–5 | 266 secs |

In Table 6 are given the extrema of velocities on the geometric centerlines of the cavity. Streamlines are drawn in figures 12-17. From these figures we distinguish easily two big vortices, one near the moving top of the cavity (called principal vortex), another, called secondary vortex, on the lower left-corner if $A > B$ and near the bottom if $A < B$. We give in table 7 the location of the center of these vortices and the corresponding value of $\Psi$.

TABLE 6

*Minimum value of u-velocity on the vertical centerline and minimum & maximum values of v-velocity on the horizontal centerline*

| $A = 1, B = 0.5$ | | | |
|---|---|---|---|
| $R$ | $u_{min}$, $y_{min}/B$ | $v_{max}$, $x_{max}/A$ | $v_{min}$, $x_{min}/A$ |
| 100 | –0.30608, 0.33125 | 0.14693, 0.14063 | –0.34645, 0.89063 |
| 1000 | –0.30056, 0.29375 | 0.35709, 0.46562 | –0.58747, 0.94062 |
| 5000 | –0.25470, 0.30625 | 0.49368, 0.48438 | –0.64159, 0.96562 |
| $A = 0.75, B = 1$ | | | |
| $R$ | $u_{min}$, $y_{min}/B$ | $v_{max}$, $x_{max}/A$ | $v_{min}$, $x_{min}/A$ |
| 100 | –0.19334, 0.60938 | 0.10836, 0.22396 | –0.11939, 0.76563 |
| 1000 | –0.39450, 0.42188 | 0.26019, 0.22396 | –0.33961, 0.79688 |
| 5000 | –0.52006, 0.39687 | 0.34351, 0.18229 | –0.41621, 0.82813 |
| $A = 0.5, B = 1$ | | | |
| $R$ | $u_{min}$, $y_{min}/B$ | $v_{max}$, $x_{max}/A$ | $v_{min}$, $x_{min}/A$ |
| 100 | –0.19157, 0.75937 | 0.02035, 0.23125 | –0.01929, 0.71875 |
| 1000 | –0.36401, 0.63437 | 0.02315, 0.85625 | –0.04459, 0.09375 |
| 5000 | –0.48608, 0.59687 | 0.03149, 0.79375 | –0.11132, 0.05625 |

TABLE 7

*Location of the center of the principal vortex and the secondary vortex and corresponding value of $\Psi$.*

| $A = 1$, $B = 0.5$ | | | | |
|---|---|---|---|---|
| | principal vortex | | secondary vortex | |
| $R$ | $\Psi$ | location | $\Psi$ | location |
| 100 | 7.627E–02 | (0.6625, 0.3250) | –3.12E–06 | (0.9813, 0.0187) |
| 1000 | 8.177E–02 | (0.7000, 0.2813) | –4.69E–03 | (0.1813, 0.2438) |
| 5000 | 8.060E–02 | (0.7188, 0.2688) | –1.19E–02 | (0.2125, 0.2563) |
| $A = 0.75$, $B = 1$ | | | | |
| | principal vortex | | secondary vortex | |
| $R$ | $\Psi$ | location | $\Psi$ | location |
| 100 | 7.717E–02 | (0.4531, 0.8125) | –1.30E–05 | (0.6719, 0.0812) |
| 1000 | 8.936E–02 | (0.3984, 0.6938) | –6.00E–03 | (0.2188, 0.2188) |
| 5000 | 9.869E–02 | (0.3906, 0.6938) | –1.11E–02 | (0.2031, 0.2250) |
| $A = 0.5$, $B = 1$ | | | | |
| | principal vortex | | secondary vortex | |
| $R$ | $\Psi$ | location | $\Psi$ | location |
| 100 | 5.089E–02 | (0.2875, 0.8750) | –1.63E–04 | (0.2625, 0.2313) |
| 1000 | 5.839E–02 | (0.2688, 0.8000) | –5.36E–03 | (0.1938, 0.4313) |
| 5000 | 6.380E–02 | (0.2563, 0.7938) | –9.48E–03 | (0.2188, 0.3750) |

## 5. CONCLUDING REMARKS

The second-order upwinding finite difference scheme presented in this paper is a very efficient one for solving the steady Navier-Stokes equations with large Reynolds numbers in the velocity-pression formulation. It is of second-order accuracy and very stable. The multigrid technique is a powerful tool for solving the discret system and the SCGS iteration proposed by S. P. Vanka provides a good smoothing operator for the multigrid solver. Numerical solutions obtained with this scheme are comparable to those obtained with second-order finite difference schemes based on stream function-vorticity formulations, both on precision and on computation time. The essential advantage of this scheme with regard to those based on the stream function is its direct applications to 3D flows and to flows with complex engineering geometries.

For the driven problem, we have obtained numerical solutions for Reynolds numbers up to 10 000. With the same MG solver and a hybrid finite-difference scheme for the descretization of the convection terms, Vanka, in [8], has declared to have difficulties with $R = 5\,000$. We think that this discrepancy may be due to the fact that the hybrid difference scheme (combination of centered and first-order upwinding differenciations) is less stable than the totally decentered differentiations used in this work.

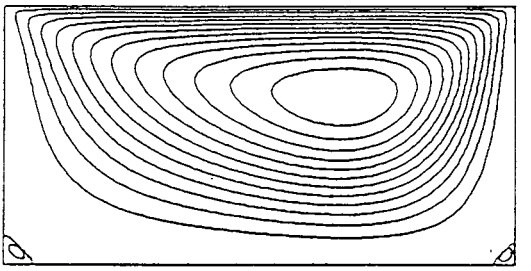

**Figure 12. — Streamlines. $A = 1$, $B = 0.5$, $R = 100$.**

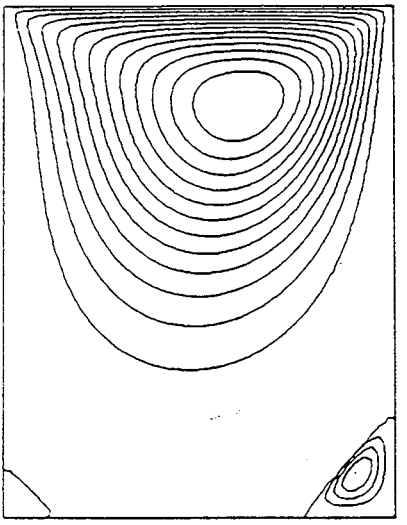

**Figure 13. — Streamlines. $A = 0.75$, $B = 1$, $R = 100$.**

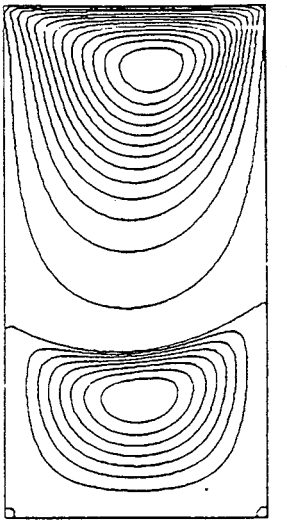

**Figure 14. — Streamlines. $A = 0.5$, $B = 1$, $R = 100$.**

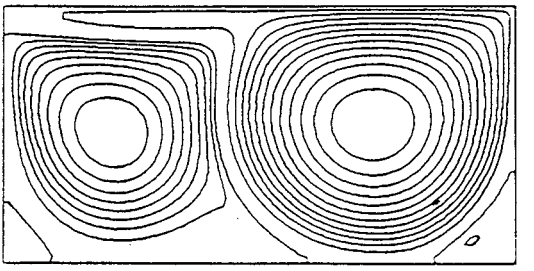

**Figure 15. — Streamlines. $A = 1$, $B = 0.5$, $R = 5\,000$.**

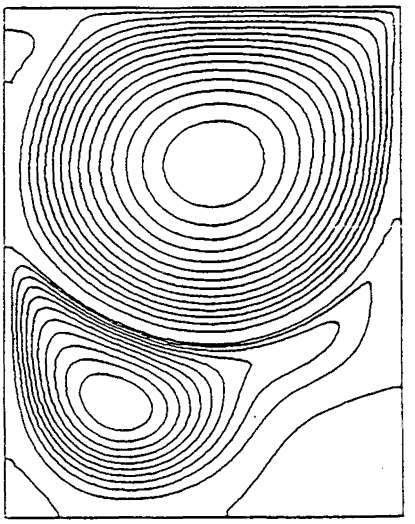

**Figure 16. — Streamlines. $A = 0.75$, $B = 1$, $R = 5\,000$.**

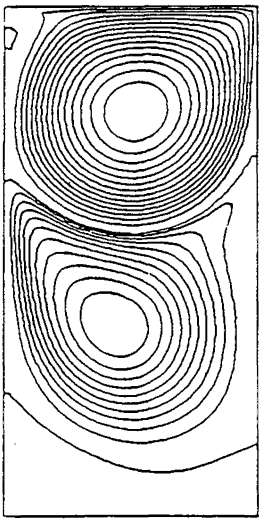

**Figure 17. — Streamlines. $A = 0.5$, $B = 1$, $R = 5\,000$.**

## REFERENCES

[1] J. D. BOZEMAN & C. DALTON, Numerical Study of Viscous Flow in a Cavity, *J. of Comp. Phys.*, 12, 1973, pp. 348-363.

[2] A. BRANDT & N. DINAR, Multigrid Solutions to Elliptic Flow Problems, *Numerical Methods in PDEs,* Ed. S. V. Parter, Academic Press, New York, 1977, pp. 53-147.

[3] Ch. H. BRUNEAU & C. JOURON, Efficient Schemes for Solving Steady Navier-Stokes Equations, *to appear.*

[4] M. FORTIN, R. PEYRET & R. TEMAM, Résolution Numérique des Équations de Navier-Stokes pour un Fluide Incompressible, *Journal de Mécanique,* Vol. 10, N° 3, septembre 1971.

[5] U. GHIA, K. N. GHIA & C. T. SHIN, High-Re Solutions for Incompressible Flows Using the Navier-Stokes Equations and a Multigrid Method, *J. of Comp. Phys.*, 48, 1982, pp. 387-411.

[6] R. SCHREIBER & H. B. KELLER, Driven Cavity Flows by Efficient Numerical Techniques, *J. of Comp. Phys.*, 49, 1983, pp. 310-333.

[7] S. Y. TUANN & M. D. OLSON, Review of Computational Methods for Recirculating Flows, *J. of Comp. Phys.*, 29, 1978, pp. 1-19.

[8] S. P. VANKA, Block Implicit Multigrid Solutions of Navier-Stokes Equations in Primitive Variables, *J. of Comp. Phys.*, 65, 1985, pp. 138-158.

[9] L. B. ZHANG, Résolution Numérique des Équations de Navier-Stokes par la Méthode Multigrille, *University Thesis,* Orsay, 1987.